Since January 2020 Elsevier has created a COVID-19 resource centre with free information in English and Mandarin on the novel coronavirus COVID-19. The COVID-19 resource centre is hosted on Elsevier Connect, the company's public news and information website.

Single-molecule conformational dynamics of viroporin ion channels regulated by lipid-protein interactions

Eneko Largo [a,b,f], María Queralt-Martín [c], Pablo Carravilla [a,b,d,e], José L. Nieva [a,b], Antonio Alcaraz [c,*]

[a] Department of Biochemistry and Molecular Biology, University of the Basque Country (UPV/EHU), P.O. Box 644, 48080 Bilbao, Spain
[b] Instituto Biofisika (UPV/EHU, CSIC), University of the Basque Country, Leioa E-48940, Spain
[c] Laboratory of Molecular Biophysics, Department of Physics, University Jaume I, 12071 Castellón, Spain
[d] Institute of Applied Optics and Biophysics, Friedrich-Schiller-University Jena, Max-Wien Platz 1, 07743 Jena, Germany
[e] Leibniz Institute of Photonic Technology, Albert Einstein Strasse 9, Jena, Germany
[f] Department of Immunology, Microbiology and Parasitology, Faculty of Medicine, University of the Basque Country (UPV/EHU), Leioa, Bizkaia, Spain

ARTICLE INFO

ABSTRACT

Classic swine fever is a highly contagious and often fatal viral disease that is caused by the classical swine fever virus (CSFV). Protein p7 of CFSV is a prototype of viroporin, a family of small, highly hydrophobic proteins postulated to modulate virus-host interactions during the processes of virus entry, replication and assembly. It has been shown that CSFV p7 displays substantial ion channel activity when incorporated into membrane systems, but a deep rationalization of the size and dynamics of the induced pores is yet to emerge. Here, we use high-resolution conductance measurements and current fluctuation analysis to demonstrate that CSFV p7 channels are ruled by equilibrium conformational dynamics involving protein-lipid interactions. Atomic force microscopy (AFM) confirms the existence of a variety of pore sizes and their tight regulation by solution pH. We conclude that p7 viroporin forms subnanometric channels involved in virus propagation, but also much larger pores (1–10 nm in diameter) with potentially significant roles in virus pathogenicity. Our findings provide new insights into the sources of noise in protein electrochemistry and demonstrate the existence of slow complex dynamics characteristic of crowded systems like biomembrane surfaces.

© 2020 Elsevier B.V. All rights reserved.

1. Introduction

Viroporins are multifunctional proteins that induce ion channel activity, a decisive function in the virus spread and pathogenicity [1,2]. Although membrane permeabilization by pore-forming proteins has been traditionally considered a very relevant phenomenon in biology [3–11], studies focused on structural combinations of lipids and viral proteins are relatively recent [12–16].

Classical swine fever (CSF) is an often lethal and highly contagious disease of swine. The etiological agent, CSF virus (CSFV), is a small enveloped virus with a positive single-stranded RNA genome that is classified as a member of the genus *Pestivirus* within the family *Flaviviridae* [17]. CSFV p7 is a viroporin that is involved in CSFV virulence [18] and is essential for virus production [19], but unfortunately its biological functions in the viral cycle and underlying mechanisms are unclear. CSFV p7 pore-forming activity [18] shows a diversity of conductance levels and lifetimes that can be relevant for permeabilization of the cell endomembranes during the replication cycle of the virus, and for the regulation of its interactions with the host [18,20]. Despite previous efforts that identified minimal conducting structures (between 0.7 nm and 1.5 nm) with opposite ion selectivities [21,22], the structural nature of CSFV p7-induced pores is still unclear. We show here the coexistence of these small configurations with other much larger structures, which could be relevant in several contexts.

From the electrophysiological aspect, different mechanisms have been invoked to describe membrane permeabilization by peptides [10,11,23–26]: proteins that assemble with lipids to form distinctive channel structures (e.g. "barrel stave" pores like Alamethicin [24] or "toroidal" pores like melittin [10,25]) versus "detergent-like mechanisms" in which proteins just disrupt the lipid packing and disintegrate the bilayer [26]. Although in the literature of ion channels formed by transmembrane proteins, "channel" and "pore" are synonyms [27], in the context of membrane-permeabilizing proteins may be a subtle distinction between these terms. Thus, the so-called "channel-pore dualism" refers to the

* Corresponding author.
   E-mail address: alcaraza@uji.es (A. Alcaraz).

hypothetical coexistence of characteristic proteolipidic "channels" showing typical ion channel features (like voltage gating and ion selectivity) and other "pores" randomly created by membrane disruption that do not show neither spontaneous closures nor ion discrimination [28,29]. In addition to that, pore formation might be also artifactual due to the application of voltage if channel formation occurs via electroporation [30,31]. On the virological side, the existence of pore structures of diverse sizes could be relevant to different stages of virus progression. Viroporin pores can help the virus enter the cell, as the Influenza virus M2 viroporin, which pemeabilizes the virus envelope under the appropriate conditions and ultimately triggers the release of the viral genome into the host cell's cytoplasm [32]. Or the SARS-CoV E viroporin, whose ion channel activity represents a key determinant for SARS-CoV virulence [1,14]. Viroporins can also promote replication without disturbing cell homeostasis, whereas large pores could be crucial to provide an exit pathway when endoplasmic reticulum (ER) disruption occurs in the pathogenic stage [33].

To probe the nature, size and possible function of CSFV p7 pores [18] we examine the open channel current noise (amplitude and frequency of current oscillations) calculating the power spectral density (PSD) of the signal together with the corresponding autocorrelation function in different conditions of pH and membrane composition. PSD is calculated via the Fourier transform of the current versus time recordings (see Materials and Methods). It has been very useful to identify the frequency hallmark of the underlying physical mechanisms responsible for pore formation in different membrane systems [34–36], among other applications [37]. Here, we use the analysis of fluctuations to identify the mechanisms of CSFV p7 pore formation and to validate the existence of different pore conformations. Detecting the sources of noise in both synthetic and biological nanopores is not only important for academic purposes, but also helps to reduce the signal-to-noise ratio determining the time resolution of experimental set-ups in bioanalytical [38] and large-scale technological applications [39]. To complement noise analysis, we analyze the effect of p7 on ER-like membranes considering the effect of solution acidity, using AFM, which provides nanometer resolution.

We conclude that p7 viroporin forms subnanometric channels like those described in previous studies, but also much larger distinct pores visible in AFM imaging. Our analysis supports that all those channels share a common source of current noise: equilibrium conformational rearrangements involving lipid-protein interactions. The capacity of viroporins to assemble pores of different sizes in membranes could be critical in subsequent stages of the process of virus replication and virulence.

2. Material and methods

2.1. Materials

The CSFV p7 protein was commercially synthesized (Thermo Scientific). Small, diluted aliquots were stored in dimethyl sulfoxide (DMSO) and frozen upon use. Dioleoyl phosphatidylcholine (PC), dioleoyl phosphatidylethanolamine (PE), liver phosphatidylinositol (PI), and dioleoyl phosphatidylserine (PS) were purchased from Avanti-Polar Lipids (Birmingham, AL).

2.2. Planar lipid membranes formation

Membrane formation was performed either with pure PS or with a mixture of PC:PE:PI 5:3:2 that emulates ER membranes [40], as indicated throughout the text. Two monolayers were made, as described previously [12], from 5 mg/ml pentane solutions of lipid mixture added at both sides of Teflon chambers filled with KCl buffered with 5 mM HEPES and partitioned by a 15 μm thick Teflon film with 70–100 μm diameter orifices. Planar lipid bilayers were formed by monolayer apposition [41] on the orifices previously treated with a 1% solution of hexadecane in pentane. Due to its high hydrophobicity, CSFV p7 protein dissolved in DMSO was supplemented to the lipid solutions at a final concentration of 250 nM prior to monolayer formation only in one of the chamber sides, referred to as cis side.

2.3. Channel conductance measurements

An electric potential was applied using Ag/AgCl electrodes in 2 M KCl, 1.5% agarose bridges assembled within standard 250 μl pipette tips. Potential is defined as positive when it is higher at the side of protein addition (the *cis* side), while the *trans* side is set to ground. An Axopatch 200B amplifier (Molecular Devices, Sunnyvale, CA) in the voltage-clamp mode was used for measuring the current and applying potential. Current was filtered with a 10 kHz 8-pole in-line Bessel filter and digitized with a Digidata 1440A (Molecular Devices, Sunnyvale, CA) at 50 kHz sampling frequency. The membrane chamber and the head stage were isolated from external noise sources with a double metal screen (Amuneal Manufacturing Corp., Philadelphia, PA).

A rough first estimation of pore diameter considered a cylindrical neutral pore. Thus, channel conductance G can be written in terms of solution conductivity κ, and pore dimensions, according to the following equation:

$$G = \frac{\pi D^2}{4L} \kappa \tag{1}$$

where L and D stand for length and diameter, respectively.

2.4. Current fluctuation analysis

The power spectral density (PSD) of current fluctuations and the normalized autocorrelation function were obtained directly from the measured current traces with the pClamp 10 software (Molecular Devices, LLC.). The power spectrum generates a frequency domain representation of the time domain data, revealing the power levels of different frequency components in the signal. PSD was measured by calculating the Fast Fourier Transform from the digitized signal without further digital filtering. The PSD spectral resolution used was 0.76 Hz and, for each signal, the available spectral segments were averaged. The normalized autocorrelation function was generated using the maximum available number of time lags for each segment. All types of CSFV p7 permeabilization events observed in the experiments were included in the current fluctuation analysis. Given that protein was supplemented to the lipid fraction *prior to* membrane formation, observed events could be divided in two main types: On one hand, some events were stable enough so voltage could be applied and removed and re-applied. These events allowed for quantification of background fluctuations (this is the case of all Figures where background noise is shown). In other occasions, current appeared during application of a constant voltage, so there was no zero level available. In this case, the current level could be stable or otherwise transition to new current levels while voltage is applied. In any case, the criterion used to define an event for noise analysis was always the same: events were restricted to sections where histrograms of current values could be represented by a single Gaussian peak. This is necessary as noise analysis requires identification of the average current of the analyzed section.

2.5. Supported lipid bilayer formation

Supported lipid bilayers (SLBs) were prepared following the vesicle fusion protocol. Small unilamellar vesicles (SUVs) were prepared by tip sonication. Briefly, 0.5 μmol of a given lipid mixture were prepared in choloroform and dried in vacuum desiccator for 1 h. Then, the dry lipid film was resuspended in 1 mL of pure water to a final concentration of 0.5 mM and subsequently tip sonicated by appliying 60 cycles of 10 s ON/10 s OFF. To prepare peptide-containing SLBs, CSFV p7 was mixed with SUVs at indicated peptide:lipid ratios for 15 min. To prepare the SLB, freshly cleaved mica was mounted on a temperature-controlling Biocell liquid cell (JPK Instruments, Germany). Then, 0.1 mL of the SUV solution were mixed with 0.25 mL of a Ca^{2+}/HBS solution (0.2 mM $CaCl_2$, 10 mM HEPES, 150 mM NaCl pH 7.4) and incubated for 1 h at 55 °C. Finally, the medium was exchanged by 10 mM sodium acetate, 150 mM KCl pH 5.0 and the bilayer left to equilibrate for 30 min. SLBs were imaged within the same day.

2.6. Atomic force microscopy measurements

Measurements were performed on a NanoWizard II AFM (JPK Instruments, Germany). The temperature in the Biocell was kept constant at 25 °C. MSNL-10 silicon nitride cantilevers (Veeco Instruments, Plainview, NY, USA) with a spring constant of 0.01–0.1 N/m and a nominal tip radious of 2 nm were used in contact scanning mode. The setpoint was kept constant to 0.1 N/m and the scanning rate adjusted between 0.5 and 2 Hz.

3. Results and discussion

### 3.1. Determination of CSFV-p7 pore size

CSFV p7 forms membrane pores displaying a multiplicity of current levels and lifetimes [21,22]. Fig. 1A shows a characteristic electrophysiological recording of CSFV p7 in 150 mM KCl and pH 5.0 in a membrane mimicking ER membranes, where the protein is predicted to insert [18]. This trace, which is representative of the majority of current recordings, contains small current jumps (several pA) over large absolute current values (hundreds of pA). In a few cases, CSFV p7-induced currents show large fluctuations (hundreds of pA) between two well-defined levels, as shown in Fig. 1B.

Histograms of current increments (Fig. 2A) provide most probable conductance (defined as G = I/V) values of $\Delta G \sim 0.1$ nS (solid line in Fig. 2A, inset) compatible with a pore radius of $r \sim 0.5$–1 nm (via Eq. (1)). Typically, the existence of single pores with conductance values around 0.1 nS is evaluated by tracking insertions from a zero-current baseline. Thus, starting at zero current (I = 0 A), successive insertions and retractions should be consistent with $\Delta G \sim 0.1$ nS, which is considered to be the *minimal unit* conductance. Conductance increments larger than this value may be described as the collective action (multiple insertions) of such minimal units [8,12].

However, in the present study it was not possible to obtain p7-induced pores via protein insertion directly from the solution into a pre-built membrane because of the high hydrophobicity of the viroporin. Permeabilization events appeared only when CSFV p7 was added to ER-like lipid mixtures (5:3:2 PC:PE:PI) *prior* to bilayer formation so that, most often, a current was immediately present when membrane was formed and voltage was applied. Therefore, within this procedure, observed currents jumps are not necessarily consecutive incorporations of minimal pore structures, because pore structures of different sizes may be pre-formed in the membrane before the application of voltage. Large currents may either reveal the existence of enormous pores, the collective action of clusters of small pores [21,22] or even the combination of both permeabilization mechanisms.

Histograms of the absolute current values depicted in Fig. 2B for the same conditions as in Fig. 2A show the most probable conductance peak at G ~ 2 nS and secondary peaks at higher conductances. These values are one/two orders of magnitude larger that the conductance increments shown in Fig. 2A, which using Eq. (1) could imply pores 5–10 times wider than the minimal single-pore unit. A high variability in pore conformations, understood in terms of both static disorder (existence of different current levels in the traces) and dynamic disorder (current levels vary with time) [42], would suggest that channels formed by p7 protein could play radically different roles at different stages of the virus life cycle.

AFM measurements were performed on ER-like supported lipid bilayers (SLBs) at pH 5.0 to directly visualize CSFV p7-induced pores (Fig. 3A, right (+CSFV p7)). AFM is a scanning probe microscopy technique that provides nanometer resolution in the *xy* axis and sub-nanometer resolution on *z*, and thus, it is ideally suited to study pore-forming proteins in planar membranes. AFM experiments demonstrate the existence of a variety of pores, including
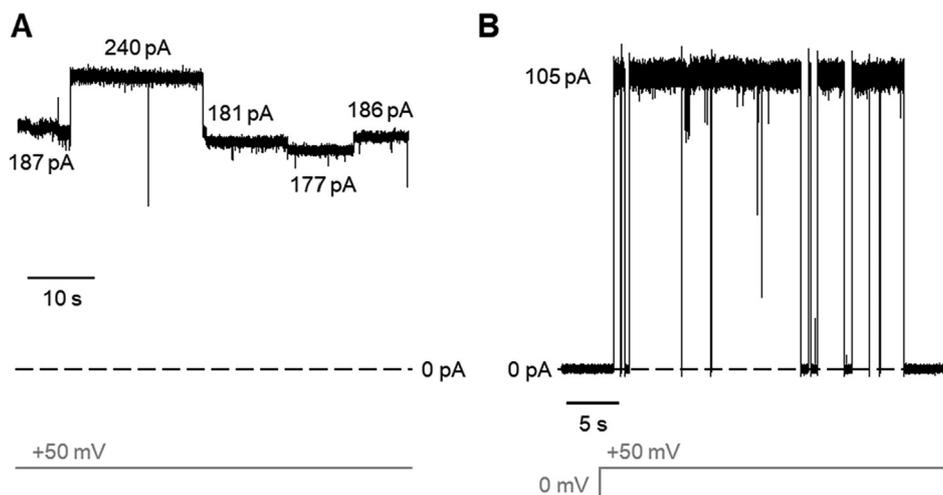
Fig. 1. CSFV p7 induces small and large current jumps. (A) Representative current trace of CSFV p7-induced pores in which small current jumps are observed over a large absolute current. (B) Example current trace in which CSFV p7 promotes large current jumps. Dashed lines indicate zero current level. Applied voltage (50 mV) is indicated as grey solid lines. Traces obtained in ER-like membranes (7:3:2 PC:PE:PI), 150 mM KCl pH 5.0 and digitally filtered at 500 Hz using a low-pass Bessel (8-pole) filter.
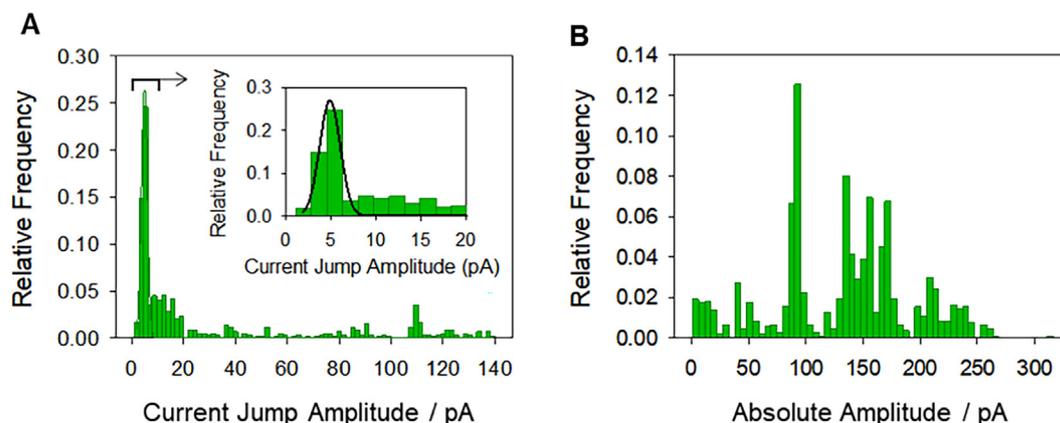
Fig. 2. CSFV p7-induced currents show small current increments as well as large absolute current values. (A) Histograms of current increments (600 events) and (B) absolute current levels (1109 events) of CSFV p7-induced currents in ER-like membranes (5:3:2 PC:PE:PI) in 150 mM KC, pH 5.0 and V = 50 mV. The inset in (A) shows a detail of the histrogram peak and its Gaussian fitting (solid line). Events were gathered from at least five independent experiments.
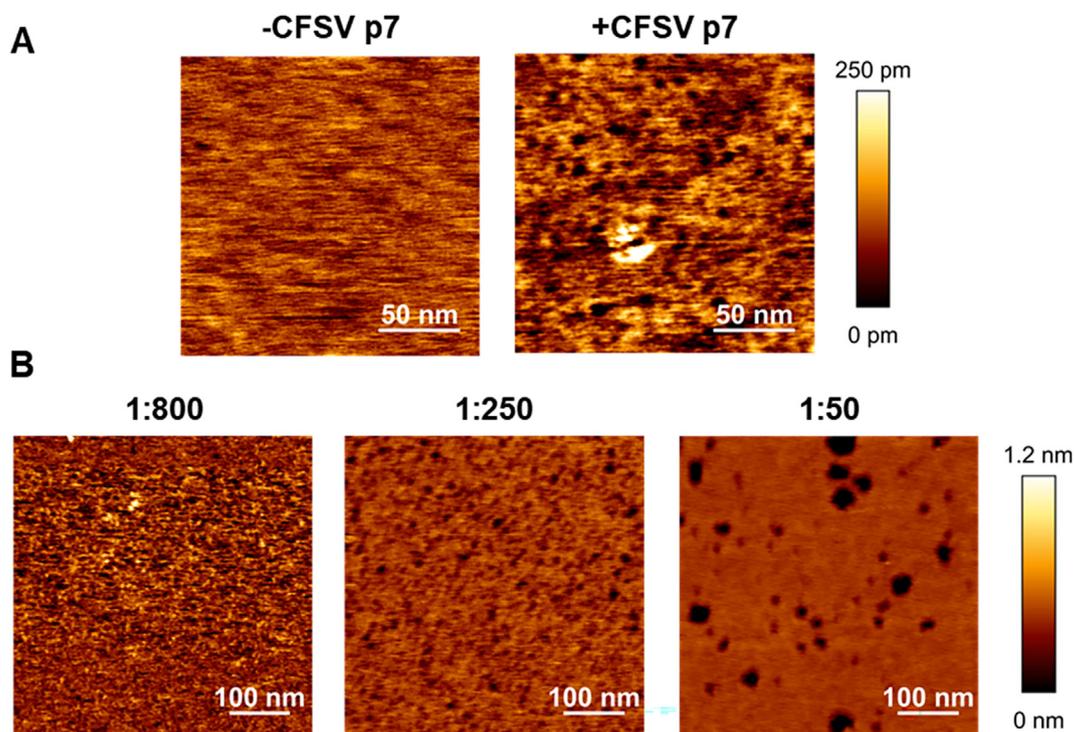

Fig. 3. CSFV p7 forms small and large pores in liposomes. (A) AFM images in ER-like liposomes at pH 5 in the absence (left) and presence (1:800 protein:lipid mol ratio, right) of CSFV p7. (B) AFM images in ER-like liposomes at pH 5 obtained using different CSFV p7:lipid ratios. Due to the membrane activity of CSFV p7, at 1:50 ratios some areas of the SLBs presented a high number of nanometric protrusions that we hypothesized to be lipid:protein aggregates (Supplemary information Fig. S1). Note that due to the shape of the AFM MSNL-10 tips, with a nominal and maximal radius of 2 nm and 12 nm respectively, the depth of pores at 1:800 ratios could not be fully resolved. The color bar indicates the height in the z dimension, being white the highest and black the lowest areas.

very large ones (radius in the order of tens of nanometers), not visible in the absence of protein (Fig. 3A, left (−CSFV p7)). Experiments performed at different lipid:protein ratios (Fig. 3B) show the dependence of pore size and number on CSFV p7 concentration, allowing for a better visualization of pores and underscoring the critical role of protein-lipid interactions. Importantly, Fig. 3 demonstrates that CSFV p7 can form a variety of pore structures in ER-like membranes in the complete absence of an applied electrical voltage, discarding electroporation (pore creation by electrical pulses) [30,31] as the only source of channel formation.

3.2. CSFV-p7 power spectra show 1/f noise compatible with conductance fluctuations

Next, we delved into the current recordings paying attention to the open channel noise and particularly to its dependence on frequency. Exploration of PSD from membrane pores has proven to be very challenging [35], due to the presence of many different contributions [43]. The PSD spectrum of membrane pores can be described as:

$$PSD = a\frac{1}{f^\alpha} + b + cf + df^2 \tag{2}$$
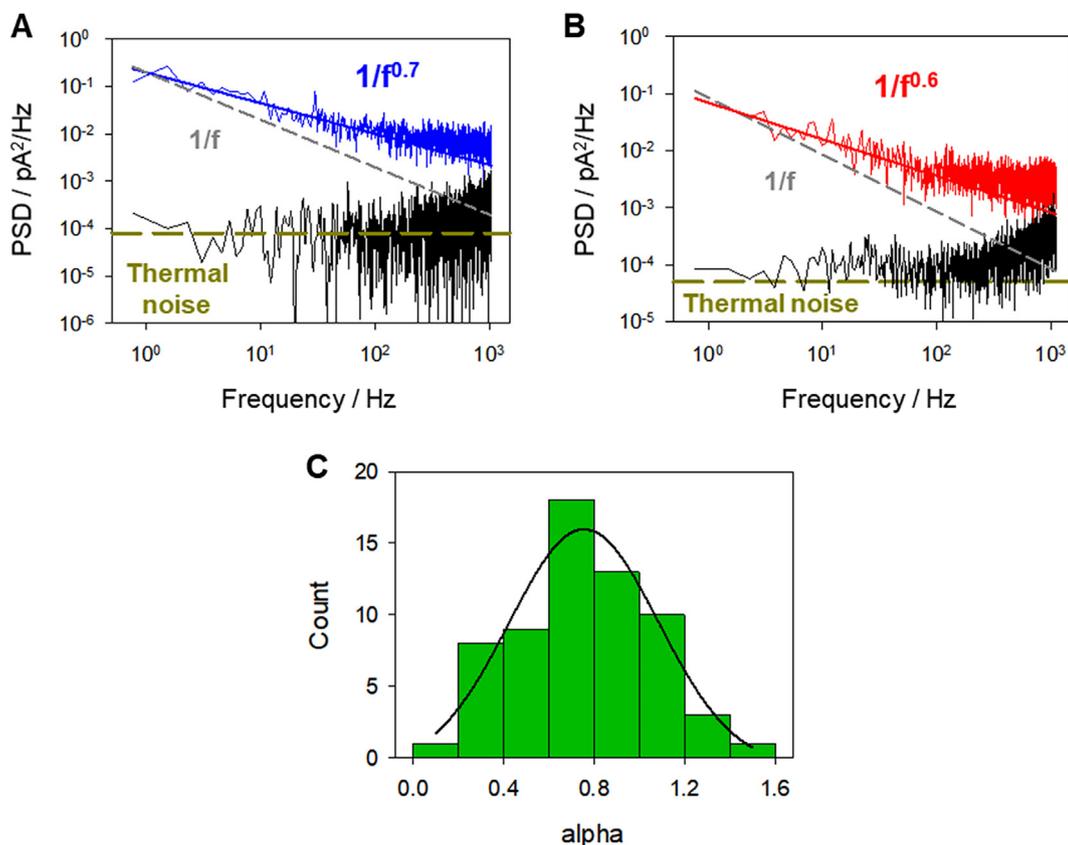
Fig. 4. CSFV p7 currents with different amplitudes show similar fluctuation patterns. (A) Power spectral density of the current trace shown in Fig. 1A (blue spectrum). Thermal noise (dark yellow dashed line) calculated as $4kTG$ using channel conductance of Fig. 1A (G ~ 4.8 nS). Background noise (black spectrum) obtained at the same conditions as in Fig. 1A with V = 0 mV. (B) Power spectral density of the current trace shown in Fig. 1B (red spectrum). Thermal noise (dark yellow dashed line) calculated as $4kTG$ using channel conductance of Fig. 1B (G ~ 2 nS). Background noise (black spectrum) obtained at the same conditions as in Fig. 1B with V = 0 mV. (C) Histograms of α from 60 CSFV p7 current traces in the same conditions as in (A-B). Events were gathered from at least five independent experiments. (For interpretation of the references to colour in this figure legend, the reader is referred to the web version of this article.)

where f is the frequency and a, b, c and d are coefficients [38,43–45]. The entire frequency range is covered by the addition of flicker noise a/f^α, white thermal noise b, dielectric noise cf and capacitive noise df^2 [43].

The white thermal noise can be calculated as $b = 4kTG$ being G the channel conductance, k the Boltzmann constant and T the absolute temperature. As regards flicker noise a/f^α, $\alpha = 0$ (actually $0 < \alpha$ less than 0.5) represents white noise ($1/f^0$) whereas $\alpha > 0.5$ is linked to different kinds of colored noise [46]. Several mechanisms can potentially generate $1/f^\alpha$ noise in the context of membrane transport, namely correlated ion jumps over a single energy barrier [34], random diffusion processes (formally equivalent to jumps in multi energy-barrier systems) [34], conformational fluctuations between different open channel sub-states [47], transitions between open and closed states [46] and even self-organized criticality [48]. Moreover, recent studies show that 1/f noise arising from confinement effects – appearing when channel dimensions are comparable to the size of the flowing particles – can induce slow dynamics, ion correlations or cooperativity in the ionic motion [39,44].

At high frequencies (f > 1 kHz), the power spectrum is dominated by thermal, dielectric and capacitive noise including those induced by the amplifier and the electrochemical cell [43]. For the sake of simplicity, we excluded from our analysis this high frequency region and focused on the nature and origin of the current fluctuations in the low frequency limit (f ≤ 1 kHz) where the contribution of membrane pores appear [43,46,49,50]. Examples of full

spectra including all effects and the final high-frequency drop generated by the low-pass Bessel filter in the amplifier are presented in Supplementary Material (Fig. S2).

Fig. 4A shows the PSD of the section of Fig. 1A where I ~ 240 pA and Fig. 4B shows the PSD of the current trace section in Fig. 1B where I ~ 105 pA. PSDs show characteristic $1/f^\alpha$ type spectra.

Interestingly, the measured background noise in the low frequency range lies on the same level as the calculated thermal noise floor for the channel conductance in each case (G ~ 4.8 nS in Fig. 4A and G ~ 2.0 nS in Fig. 4B). Also remarkably, PSDs deviate significantly from 1/f noise (shown in grey in each figure), so that we get α ~ 0.7 for the blue spectrum in Fig. 4A and α ~ 0.6 for the red one in Fig. 4B when fitting $1/f^\alpha$ to the measured PSD in the range 0.1–20 Hz. Spectra shown in Fig. 4A and B are representative of the overall situation. A histogram of alphas obtained from different current traces is shown in Fig. 4C, the most probable value being $\alpha = 0.75 \pm 0.25$.

Data displayed in Fig. 4 raise some questions concerning the nature of pores and the origin of current fluctuations. On the one side, despite Fig. 3 showing CSFV p7-induced pores without applied voltage, it is still unclear if recorded channels could partially arise from electroporation due to the applied voltage [30,31]. Another issue is the possible occurrence of the channel-pore dualism mentioned before. In such case, the small structurally well-defined pore structures characteristic of the perforating protein (CSFV p7 in this case), would coexist with larger holes, resulting from the membrane disruption generated by a potential

detergent-like action of the protein [26]. Exploring how noise depends on applied voltage, lipid composition and protein titration by pH may provide new insights into such questions.

Thus, we next analyzed relatively stable current traces (i.e. the histogram of current values can be represented by a single peak) of the CSFV p7 protein at different applied potentials. Fig. 5A displays a linear I-V relationship where the total conductance is G ~ 3 nS. The corresponding PSD is shown in Fig. 5B.

In Fig. 5B, the magnitude of the applied potential determines the absolute value of noise, but not the slope in the calculated PSD (all spectra at V $\neq$ 0 have a similar slope). In both polarities, measured spectra scale approximately as $1/f^{0.5}$ and spectral density is considerably higher than the background noise (V = 0 mV).

Fig. 5C shows that PSD at 1 Hz (PSD_{1Hz}) obtained from the spectra in Fig. 5B follows a parabolic dependence on applied voltage, a distinctive feature of equilibrium conductance fluctuations [47,51], which is different from the patterns found in electroporation in planar lipid bilayers [52], and from the non-equilibrium 1/f fluctuations observed in rectifying nanopores [53]. Current traces with smaller conductance levels than those reported in the top panels also display equilibrium conductance fluctuations (Fig. 5D–F). Fig. 5D shows an I-V curve with ohmic behavior (G ~ 0.35 ns), being the corresponding PSD, shown in Fig. 5E, closer to the level of background noise and the $1/f^{\alpha}$ behavior (α ~ 0.4) restricted to lower frequencies. Interestingly, calculated PSD_{1Hz} (Fig. 5F) displais quadratic dependence on V pointing again to equilibrium conductance fluctuations. Therefore, the data displayed in Fig. 5 demonstrates the existence of a common mechanism for noise generation in either large or small currents. This indicates that

CSFV p7 is capable of forming a variety of pores with different sizes, and these structures have similar dynamical properties of equilibrium nature regardless of their size, suggesting not only that electroporation does not occur, but also that no "channel-pore" dualism is present.

3.3. Random transitions as a mechanism for $1/f^{\alpha}$ noise

Many studies in biological and synthetic membrane systems show equilibrium conductance noise in which the amplitude of the 1/f power law increases as the square of the average current [44–46]. Such oscillations may arise either from changes in pore geometry [46,47] or from fluctuations in charge carrier concentration [51,54].

In a seminal paper, Bezrukov and Winterhalter attributed the origin of 1/f noise in a protein channel (maltoporin) to random transitions between different conducting sub-states of the open pore [47]. It was shown that if current steps are excised using a special algorithm, the PSD of the resulting current becomes almost flat (white noise, α ~ 0). This effect was independent of the pore size. Fig. 6 indicates that this mechanism could also operate in CSFV p7 channels in ER-like membranes. Fig. 6A shows a trace with a well-defined conductance level that can be described with a single peak (indeed, it is the trace corresponding to V = 50 mV in Fig. 5A). The corresponding spectrum, in red in Fig. 6B, shows $1/f^{\alpha}$ noise with α ~ 1.5. However, we can calculate again the PSD but excluding the small current jumps (blue spectrum in Fig. 6B) so that the power spectrum shows almost white noise (α ~ 0.3), as predicted by Bezrukov and colleagues [47]. This kind of beha-
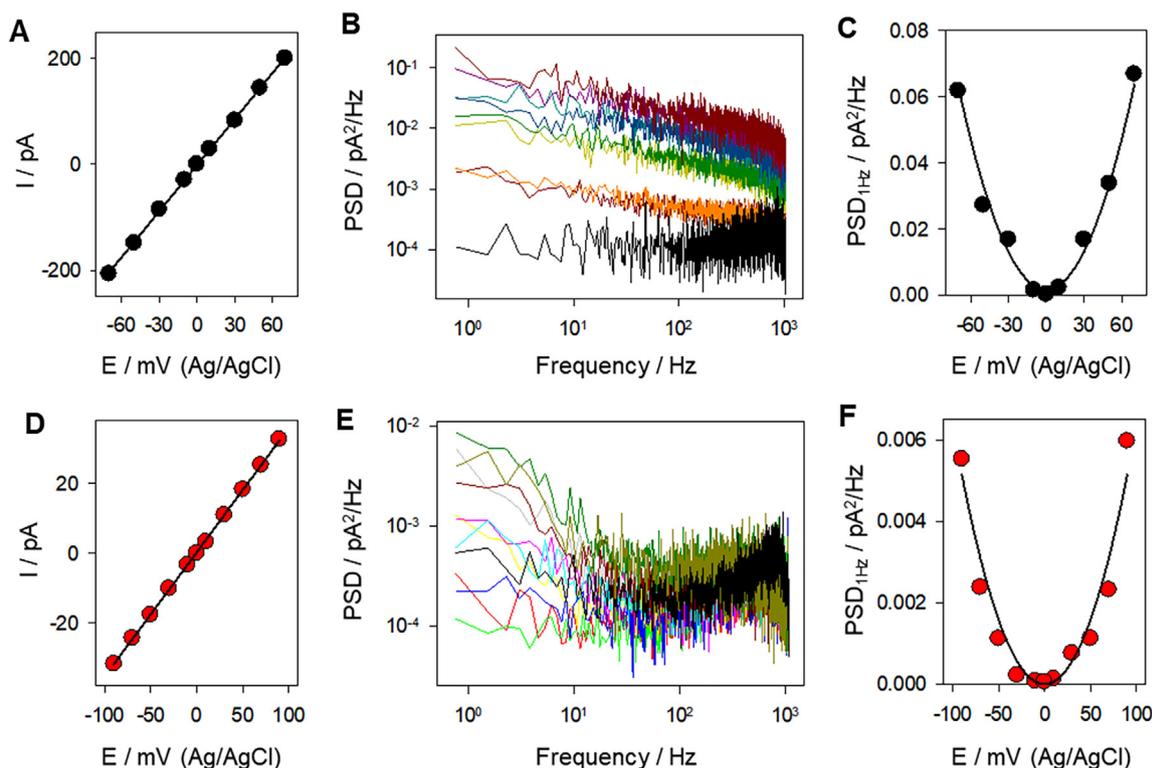
Fig. 5. CSFV p7-induced currents are Ohmic and display equilibrium conductance fluctuations. (A) Current-voltage curve obtained from current trace of G = 3 nS. Solid line represents a linear fitting. (B) PSD as a function of frequency from the currents of panel (A). Each curve corresponds to a different applied voltage, with 0 mV (black), +10 mV (brown), −10 mV (orange), +30 mV (green), −30 mV (yellow), +50 mV (light blue), −50 mV (dark blue), +70 mV (dark red), −70 mV (purple). (C) PSD at 1 Hz obtained from (B) as a function of voltage. Solid lines represent a parabolic fitting. (D) Current-voltage curve obtained from current trace of G = 0.35 nS. Solid line represents a linear fitting. (E) PSD as a function of frequency from the currents of panel (D). Each curve corresponds to a different applied voltage, with 0 mV (black), +10 mV (red), −10 mV (light green), +30 mV (light yellow), −30 mV (blue), +50 mV (pink), −50 mV (cyan), +70 mV (brown), −70 mV (gray), +90 mV (dark green), −90 mV (dark yellow). (F) PSD at 1 Hz obtained from (E) as a function of voltage. Solid lines represent a parabolic fitting. (For interpretation of the references to colour in this figure legend, the reader is referred to the web version of this article.)
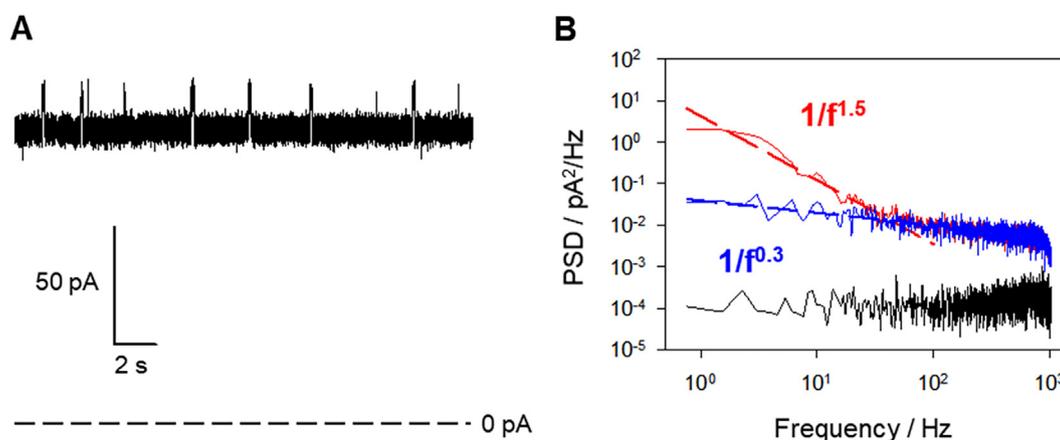
Fig. 6. Fluctuations between levels increase the slope of PSD at low frequencies. (A) Example of current trace of CSFV p7 in ER-like membranes at pH 5.0 and 150 mM KCl showing flickering between two defined levels. (B) PSD of the current trace of panel (A) includind current steps (red) and excluding them (blue). (For interpretation of the references to colour in this figure legend, the reader is referred to the web version of this article.)

viour is observed frequently in CSFV p7 electrophysiological recordings in ER-like membranes. Within the same current trace, sections with intense flickering show higher α exponents than quiet sections, but if current steps are excluded from the noisy sections the new PSD becomes comparable to that of quiet ones, with a lower exponent α but still having α > 0 (see supplementary information Fig. S3 for another example).

The physical mechanisms behind the "random transitions" of current have been described either as conformational changes within a formed channel (the so-called "channel breathing" [47]) or as the diffusion of proteins in the membrane encompassing translational or rotational motions of the whole pore structure [35,55]. The scenario here is more complex than in pure proteinaceous pores like toxins [47] or bacterial channels [55] because CSFV p7 pores are likely proteolipidic structures [21,22] and therefore, the process of pore formation involves the collective motion (diffusion in the membrane plane) and packing of both proteins and lipids. In any case, a high variety of potential channel structures in terms of geometry and dynamics would likely be the breeding ground for the occurrence of random fluctuations between different conducting levels.

3.4. Current fluctuations depend on lipid composition

It has been shown that ion channel activity of CSFV p7 is strongly dependent on lipid composition, being possible to abrogate pore formation in absence of charged lipids or in presence of cholesterol [21]. Interestingly, the variety in pore conductance values of CSFV p7 protein shown in previous sections is not a distinctive feature of ER-like membranes, similar results were obtained using a variety of lipid compositions that differed slightly from the canonical ratio 5:3:2 (PC:PE:PI) [21]. Having in mind that charged lipids are necessary to observe ion channel activity in CSFV p7 [21], we decided to explore a fully charged membrane such as DOPS extensively used in proteolipidic systems [6,8,12–14]. Histograms of the recordings measured perfomed in DOPS under the same conditions as in Fig. 2 (150 mM KCl and pH 5.0) show also a diversity of current levels (see Supplementary information Fig. S4). This observation leads to the question of whether current fluctuations depend as well so strongly on lipid composition.

A visual inspection of current traces indicates that CSFV p7 pores in ER-like membranes are considerably quieter and more stable than pores of similar conductance formed in DOPS membranes. An example of this behaviour is shown in Fig. 7A (ER-like) and Fig. 7B (DOPS). These differences are reflected in the corresponding PSD, which shows a different amplitude (quantified as PSD at 1 Hz, PSD_{1Hz}) and slope α, as shown in Fig. 7C and D, respectively, for 80–60 different current traces in ER-like (green) and DOPS (pink) membranes. For PSD_{1Hz}, the mean value obtained with DOPS is three orders of magnitude larger than that for ER-like membranes.

As regards the parameter α in the $1/f^\alpha$ spectra, Fig. 7D shows values of α = 1.21 ± 0.20 for DOPS and α = 0.75 ± 0.25 in the case of ER-like membranes. Of note, PSD_{1Hz} in DOPS membranes also shows quadratic dependence on the applied voltage (Supplementary Material, Fig. S5), pointing again to equilibrium conductance fluctuations like in ER-like membranes.

To graphically illustrate our findings, we compare two different traces, one in ER-like membranes (green) and one measured in DOPS (pink) (Fig. 8A). Both traces have similar average currents (~140 pA at + 50 mV), but DOPS trace is visually much noisier than ER-like one and even random transitions could be guessed. However, current histograms (Fig. 8A, lower panels) show a unique well-defined peak in both cases, being the one obtained in DOPS shorter and broader indicating a larger dispersion. The corresponding PSD spectra (Fig. 8B) yield α = 0.3 and α = 1.0 for ER-like and DOPS membranes, respectively. ER-like membranes seem to stabilize the protein-lipid assembly giving rise to quieter and more stable pores with current noise closer to white noise than those found in DOPS membranes. DOPS membranes are fully made of phospholipid bearing net negative charge, whereas ER-like membranes have only 20 mol% of charged lipids. We hypothesize that an "excess" of negative charge could be counterproductive for the purpose of pore formation, and that the ER membrane provides a more favorable environment.

3.5. Current fluctuations in ER-like membranes are pH-regulated

Ion channel activity of CSFV p7 in ER-like membranes is controlled by solution pH [21]. Both electrophysiological recordings and vesicle permeability assays show that the intense poration activity (90% of the experiments) detected at pH 5.0 is severely reduced (less than 10% of the experiments) at pH 7.4 [21]. AFM measurements of CSFV p7 in lipid bilayers at pH 5.0 (Fig. 3A) display a variety of pore sizes. However, pores are rarely observed when the pH is increased to 7.4 (Fig. 9) consistent with the dependence on pH of CFSV p7 pore formation.
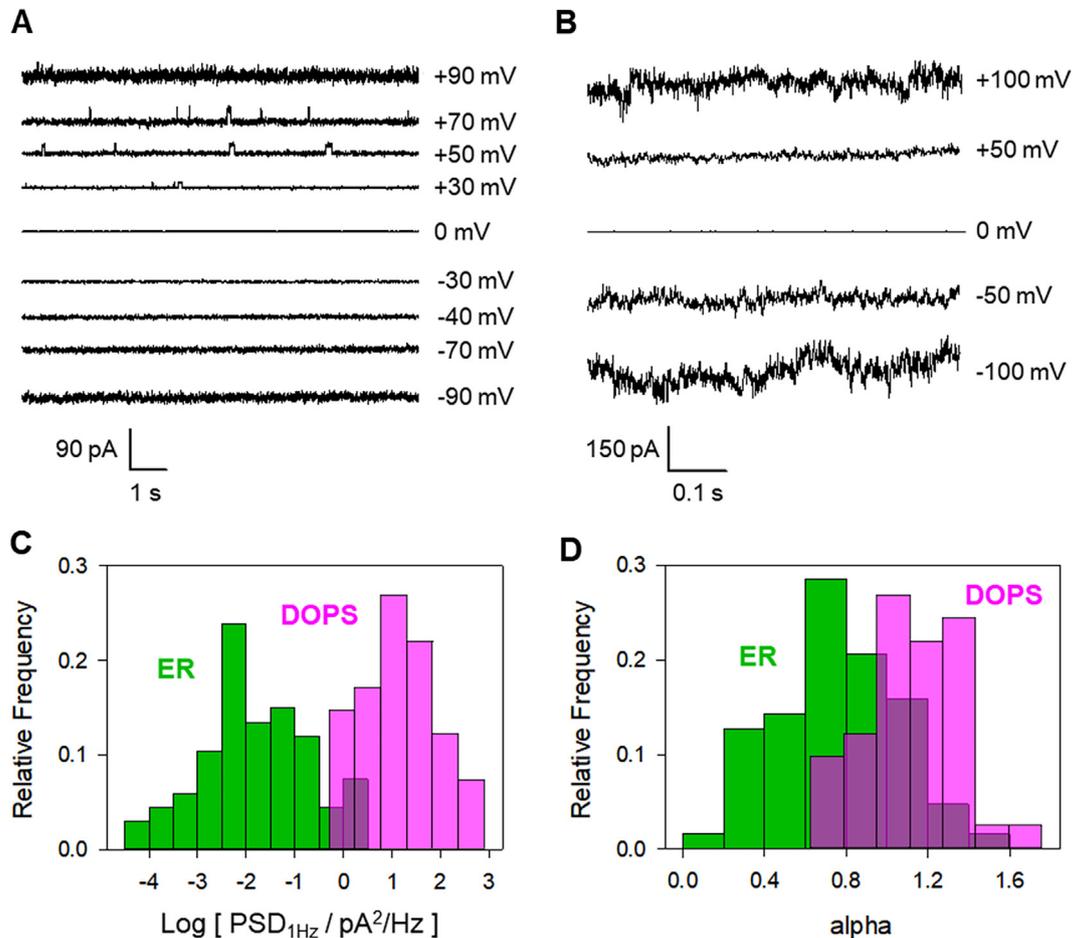
Fig. 7. CSFV p7 pores formed in ER-like membranes are considerably quieter and more stable than pores of similar conductance formed in DOPS membranes. Representative current traces of CSFV p7 pores in ER-like (A) and DOPS (B) membranes. Histograms of PSD(1 Hz) (C) and α (D) for ER-like membranes (green) and DOPS membranes (pink) at pH 5 and 150 mM KCl. Data is gathered from 60 to 80 different events obtained in at least five independent experiments. (For interpretation of the references to colour in this figure legend, the reader is referred to the web version of this article.)
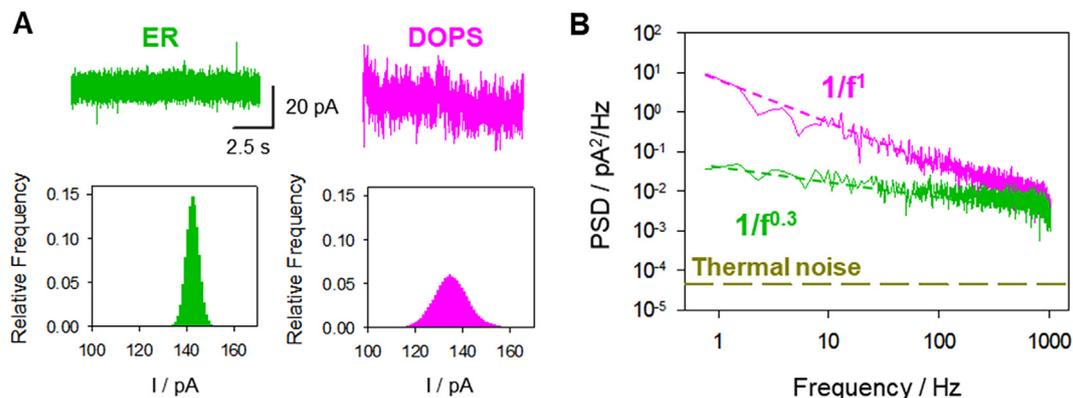

Fig. 8. (A) Current traces of CSFV p7 at pH 5 and 150 mM KCl in an ER-like membrane (green) and DOPS membrane (pink) at + 50 mV. (B) PSD of the corresponding current traces of panel (A) with the same color codes. Thermal noise (dark yellow dashed line) was calculated as $4kTG$ using a channel conductance of G ~ 2.8 nS. (For interpretation of the references to colour in this figure legend, the reader is referred to the web version of this article.)

To study the nature of small pores appearing at pH 7.4, we analyzed the current fluctuations of the residual traces obtained in these conditions, revealing that noise is also pH-dependent. Fig. 10A shows representative traces of CSFV p7 residual poration activity measured at pH 7.4 (blue), compared with traces with similar absolute current (~65 pA at +50 mV) for pH 5.0 (green). Traces

at pH 7.4 are much noisier than at pH 5.0 as clearly reflected in the current histograms, which in both cases give a unique peak but with broader distributions for pH 7.4.

Such contrasting current oscillations give rise to different PSD, as shown in Fig. 10B. In both cases, calculated PSDs give $1/f^{\alpha}$ noise, being $\alpha = 1.0$ at pH 7.4 and $\alpha = 0.3$ at pH 5.0. Traces and PSDs
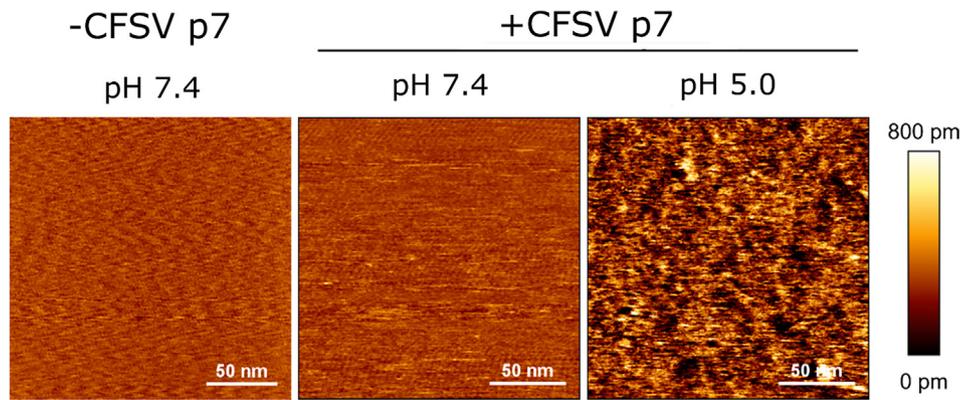
Fig. 9. The pore forming activity of CFSV p7 is reduced at pH 7.4. AFM images in ER-like lipid bilayers at pH 7.4 in control conditions (left) and in the presence of CSFV p7 at pH 7.4 (centre) and pH 5.0 (right). CFSV p7:lipid ratio was 1:800. The color bar indicates the height in the z dimension, being white the highest and black the lowest areas.
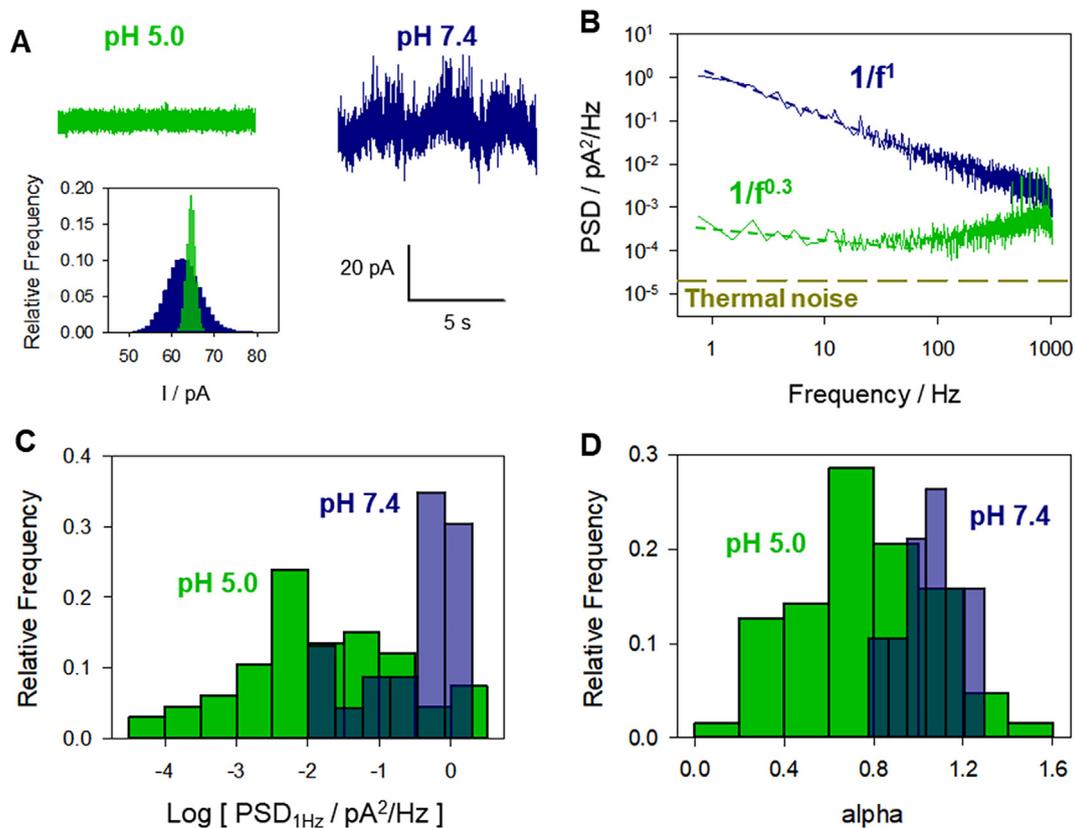

Fig. 10. pH controls noise levels in CSFV p7 pores (A) CSFB p7 representative current traces at pH 5.0 (green) and pH 7.4 (dark blue) corresponding to similar absolute current levels (~65 pA at + 50 mV). Membranes were formed with ER-like lipid in 150 mM KCl. (B) Corresponding PSD with the same color codes. Thermal noise (dark yellow dashed line) was calculated as 4kTG using a channel conductance of 1.3 nS. (C-D) Histograms of PSD(1 Hz) (C) and α (D) for CSFV p7 current traces in ER-like membranes at pH 5 (green) and pH 7.4 (blue). Applied voltage mas + 50 mV and bathing solution 150 mM KCl. Data is gathered from ~ 100 different events obtained in at least five independent experiments. (For interpretation of the references to colour in this figure legend, the reader is referred to the web version of this article.)

shown in Fig. 10A–B are representative of the overall situation, as depicted from histograms in Fig. 10C–D. Noisier traces at pH 7.4 (with respect to pH 5.0) result into higher absolute values of PSD_{1Hz} (Fig. 10C) and higher values of α (α = 1.03 ± 0.17 at pH 7.4 versus α = 0.75 ± 0.25 at pH 5.0) (Fig. 10D). These data suggest that the pH increase promoting the ionization of two histidines, which are key in forming the proteolipidic pore structures induced by p7 [21], decreases pore stability. As in the experimental case illustrated in Fig. 8, an excess of negative charge (now in the pro-

tein instead of the lipid) seems to disfavour the stability of lipid-protein assemblies.

3.6. Autocorrelation functions and pore dynamics

To evaluate the different dynamics controlling current fluctuations, we next analyzed the electrophysiological recordings focusing on the time-dependent autocorrelation function of the current traces, this is to say $i(\tau)$ = <I(t)·I(t+τ)> − <I>^{2}. Note that PSD and
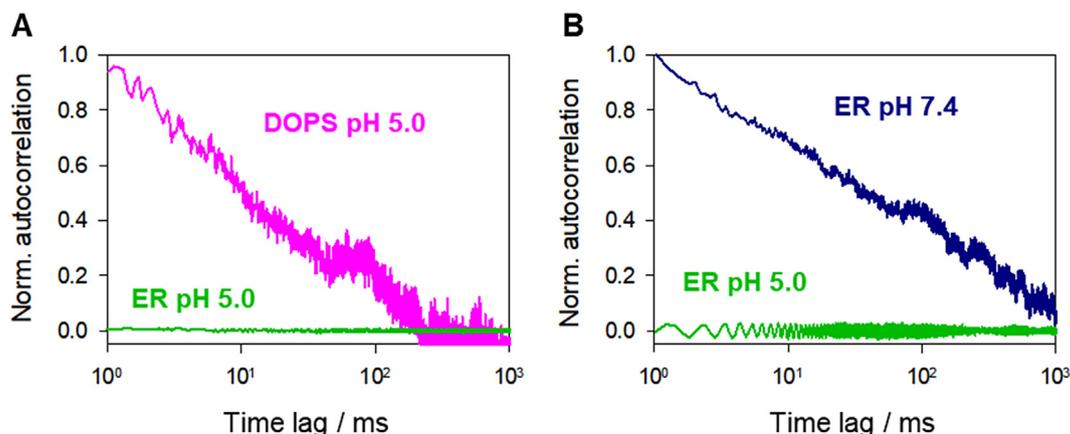
Fig. 11. Membrane composition and solution pH modulate the dynamics of current fluctuations in CSFV p7 pores. (A) Normalized autocorrelation functions ($\langle I(t) \cdot I(t+\tau) \rangle - \langle I \rangle^2)/\langle I \rangle^2$ corresponding to traces in Fig. 7A and 7B. recorded at V = +50 mV in ER-like and DOPS lipid membranes, respectively. (B) Normalized autocorrelation functions corresponding to traces in Fig. 10A recorded in ER-like membranes at pH 5.0 and 7.4.

autocorrelations are related to each other by a simple transformation and therefore contain the same information. The reason to include autocorrelations here is to provide a direct comparison with previous studies dealing with the assembly of functional proteolipidic pores [36].

First, we consider how lipid characteristics determine current fluctuations at pH 5.0. Fig. 11A shows normalized autocorrelation functions of the current traces of CSFV p7 in ER-like and DOPS membranes previously shown in Fig. 8A. Autocorrelation functions do not present a unique well-defined characteristic time, in agreement with the calculated 1/f-type PSD in Fig. 8B. The green curve (ER-like membrane) displays an autocorrelation approximately equal to zero as expected from the low value of alpha obtained in the corresponding PSD. In contrast, the pink curve (DOPS membrane) exhibits a much slower relaxation of correlations that extend to the range of seconds. As already shown in Fig. 8, changing lipid composition from ER-like to DOPS alters significantly lipid-protein dynamics and consequently the level of noise of the open pores. Note that DOPS and ER-like membranes differ fundamentally in charge (100% vs 20% in charged lipids) but also in the intrinsic curvature (PE, present at a 30 mol % in the ER-like composition, might promote non-lamellar structures [56]).

As regards pH titration, Fig. 11B shows the autocorrelation functions of the current traces reported in Fig. 10A. In agreement with PSDs shown in Fig. 10B, the low correlation observed at pH 5.0 contrasts with the slow decay observed at pH 7.4, similar to that observed in DOPS membranes in Fig. 11A. Now, it is not the lipid characteristics (lipid charge in ER-like membranes is unaltered by the pH shift from 5.0 to 7.4) but is the ionization of key acidic residues what alters the protein-lipid interactions. The change in pH not only hinders pore formation but also promotes vivid fluctuations of the pore once formed.

The slow power law decrease observed in the autocorrelation functions both in DOPS at pH 5.0 and ER-like at pH 7.4 ($\sim t^{-0.4}$, see Supplementary Information, Fig. S6) are compatible with the $t^{-1/2}$ law for approach to the jamming limit [57] characteristic of the random sequential adsorption (RSA), a model used to describe protein adsorption on nanostructured surfaces [36,58,59]. Here, the presence of slow dynamics may reflect the collective motion of proteins and lipids occurring in an extremely crowded surface similar to that of jammed systems [36], but also the enhanced packing process [58] that requires the formation of a proteolipidic pore structure.

We envisage pore formation like a multi-step process in which proteins and lipids move across the membrane surface, meet in a proper proportion and orientation and undergo the packing process that results in a transmembrane channel. Factors like lipid composition, solution pH and others (protein intrinsic characteristics) determine not only the geometry of the resulting pore but also its dynamics. The "jamming" process is visible as slow dynamics when becomes rate-limiting in the overall process of pore formation, as could happen in the slow power laws of Fig. 11A and Fig. 11B (reflected as higher values of α in PSDs of Fig. 8 and Fig. 10). In contrast, we hypothesize that these slow dynamics do not appear in ER at pH 5.0 because under these conditions the collective motion of proteins and lipids is fast enough to be non-rate-determining.

4. Conclusions

By combining electrophysiological analysis and AFM, we have shown that CSFV p7 viroporin forms pores with sizes extending from fractions to tens of nanometers in radius. While formation of small pores is a common feature of viroporins [6,9,12,15,21,32,60] (among many others), the existence of larger pores has only been inferred in specific cases [21,61]. Analysis of PSD of the current traces shows that flicker 1/f-type noise corresponds to equilibrium conductance fluctuations discarding electroporation as the channel-forming mechanism. As regards the origin of flicker noise, we have found that besides the random transitions between different conducting levels [47], additional low-frequency (slow dynamics) sources of noise appear in relation to the process of pore formation (either in the collective motion or in the membrane packing of proteins and lipids). Lipid and protein charges appear to critically regulate this conformational dynamics, as revealed by autocorrelation functions. The capital role of protein charges in channel formation and current noise when formed demonstrates that CSFV p7 forms distinctive proteolipidic channels, rather than "non-pore" arbitrary membrane disruptions. In particular, ER-like membranes at pH 5.0 display a remarkable ability to stabilize protein-lipid joint structures together with CSFV p7, providing relatively quiet pores that show low levels of flicker noise.

The findings derived from our analyses can help to understand the general functions that viroporins perform during the viral infective cycle: some of a regulatory nature and others perhaps more structural. Thus, it has been argued that the discharge of cal-

cium deposits through ER permeabilization can interfere with the cellular signaling processes that activate apoptosis [60]. This event would be mediated by stable, structurally defined and small-sized pores, and take place in the early stages of replication. The assembly of larger pores probably requires the massive expression of the protein and its incorporation in large doses into the cell endomembranes. The generation of large membrane lesions by these structures would likely occur in the final stages of the cycle, coupled with the assembly and spread of the new virions. Our quantitative analysis based on the study of current fluctuations contributes to the fine definition of these common structure–function relationships, which in turn may inform the general design of new vaccines and antivirals.

Declaration of Competing Interest

The authors declare that they have no known competing financial interests or personal relationships that could have appeared to influence the work reported in this paper.

Acknowledgements

Appendix A. Supplementary material

Supplementary data to this article can be found online at https://doi.org/10.1016/j.bioelechem.2020.107641.

References

[1] J. Nieto-Torres, C. Verdiá-Báguena, C. Castaño-Rodriguez, V. Aguilella, L. Enjuanes, Relevance of viroporin ion channel activity on viral replication and pathogenesis, Viruses 7 (2015) 3552–3573, https://doi.org/10.3390/v7072786.

[2] J.L. Nieva, V. Madan, L. Carrasco, Viroporins: structure and biological functions, Nat. Rev. Microbiol. 10 (2012) 563–574, https://doi.org/10.1038/nrmicro2820.

[3] G. Menestrina, C.L. Bashford, C.A. Pasternak, Pore-forming toxins: Experiments with S. aureus α-toxin, C. perfringens θ-toxin and E. coli haemolysin in lipid bilayers, liposomes and intact cells, Toxicon. 28 (1990) 477–491, https://doi.org/10.1016/0041-0101(90)90292-F.

[4] R.J.C. Gilbert, Pore-forming toxins, Cell. Mol. Life Sci. 59 (2002) 832–844, https://doi.org/10.1007/s00018-002-8471-1.

[5] R.J.C. Gilbert, Protein–lipid interactions and non-lamellar lipidic structures in membrane pore formation and membrane fusion, Biochim. Biophys. Acta - Biomembr. 2016 (1858) 487–499, https://doi.org/10.1016/j.bbamem.2015.11.026.

[6] E. Parra, A. Alcaraz, A. Cruz, V.M. Aguilella, J. Pérez-Gil, Hydrophobic pulmonary surfactant proteins SP-B and SP-C induce pore formation in planar lipid membranes: evidence for proteolipid pores, Biophys. J. 104 (2013) 146–155, https://doi.org/10.1016/j.bpj.2012.11.014.

[7] M.W. Parker, S.C. Feil, Pore-forming protein toxins: from structure to function, Prog. Biophys. Mol. Biol. 88 (2005) 91–142, https://doi.org/10.1016/j.pbiomolbio.2004.01.009.

[8] V.V. Malev, L.V. Schagina, P.A. Gurnev, J.Y. Takemoto, E.M. Nestorovich, S.M. Bezrukov, Syringomycin E channel: a lipidic pore stabilized by lipopeptide?, Biophys. J. 82 (2002) 1985–1994, https://doi.org/10.1016/S0006-3495(02)75547-1.

[9] U. Ros, A.J. García-Sáez, More than a pore: the interplay of pore-forming proteins and lipid membranes, J. Membr. Biol. 248 (2015) 545–561, https://doi.org/10.1007/s00232-015-9820-y.

[10] R.J.C. Gilbert, M.D. Serra, C.J. Froelich, M.I. Wallace, G. Anderluh, Membrane pore formation at protein-lipid interfaces, Trends Biochem. Sci. 39 (2014) 510–516, https://doi.org/10.1016/j.tibs.2014.09.002.

[11] J.M. Whitlock, H.C. Hartzell, A Pore Idea: the ion conduction pathway of TMEM16/ANO proteins is composed partly of lipid, Pflugers Arch. Eur. J. Physiol. 468 (2016) 455–473, https://doi.org/10.1007/s00424-015-1777-2.

[12] C. Verdiá-Báguena, J.L. Nieto-Torres, A. Alcaraz, M.L. DeDiego, J. Torres, V.M. Aguilella, L. Enjuanes, Coronavirus E protein forms ion channels with functionally and structurally-involved membrane lipids, Virology. 432 (2012) 485–494, https://doi.org/10.1016/j.virol.2012.07.005.

[13] C. Verdiá-Báguena, J.L. Nieto-Torres, A. Alcaraz, M.L. DeDiego, L. Enjuanes, V.M. Aguilella, Analysis of SARS-CoV E protein ion channel activity by tuning the protein and lipid charge, Biochim. Biophys. Acta - Biomembr. 2013 (1828) 2026–2031, https://doi.org/10.1016/j.bbamem.2013.05.008.

[14] J.L. Nieto-Torres, M.L. DeDiego, C. Verdiá-Báguena, J.M. Jimenez-Guardeño, J.A. Regla-Nava, R. Fernandez-Delgado, C. Castaño-Rodriguez, A. Alcaraz, J. Torres, V. M. Aguilella, L. Enjuanes, Severe acute respiratory syndrome coronavirus envelope protein ion channel activity promotes virus fitness and pathogenesis, PLoS Pathog. 10 (2014), https://doi.org/10.1371/journal.ppat.1004077 e1004077.

[15] W. Surya, Y. Li, C. Verdià-Bàguena, V.M. Aguilella, J. Torres, MERS coronavirus envelope protein has a single transmembrane domain that forms pentameric ion channels, Virus Res. 201 (2015) 61–66, https://doi.org/10.1016/j.virusres.2015.02.023.

[16] D.P. Gladue, E. Largo, I. de la Arada, V.M. Aguilella, A. Alcaraz, J.L.R. Arrondo, L. G. Holinka, E. Brocchi, E. Ramirez-Medina, E.A. Vuono, K.A. Berggren, C. Carrillo, J.L. Nieva, M.V. Borca, Molecular characterization of the viroporin function of foot-and-mouth disease virus nonstructural protein 2B, J. Virol. 92 (2018), https://doi.org/10.1128/jvi.01360-18.

[17] P. Becher, R. Avalos Ramirez, M. Orlich, S. Cedillo Rosales, M. König, M. Schweizer, H. Stalder, H. Schirrmeier, H.-J. Thiel, Genetic and antigenic characterization of novel pestivirus genotypes: implications for classification, Virology. 311 (2003) 96–104, https://doi.org/10.1016/S0042-6822(03)00192-2.

[18] D.P. Gladue, L.G. Holinka, E. Largo, I. Fernandez Sainz, C. Carrillo, V. O'Donnell, R. Baker-Branstetter, Z. Lu, X. Ambroggio, G.R. Risatti, J.L. Nieva, M.V. Borca, Classical swine fever virus p7 protein is a viroporin involved in virulence in swine, J. Virol. 86 (2012) 6778–6791, https://doi.org/10.1128/jvi.00560-12.

[19] C. Zhao, X. Shen, R. Wu, L. Li, Z. Pan, Classical swine fever virus nonstructural protein p7 modulates infectious virus production, Sci. Rep. 7 (2017) 12995, https://doi.org/10.1038/s41598-017-13352-w.

[20] D. Gladue, E. Largo, L. Holinka, E. Ramirez-Medina, E. Vuono, K. Berggren, G. Risatti, J. Nieva, M. Borca, Classical swine fever virus p7 protein interacts with host protein CAMLG and regulates calcium permeability at the endoplasmic reticulum, Viruses. 10 (2018) 460, https://doi.org/10.3390/v10090460.

[21] E. Largo, C. Verdiá-Báguena, V.M. Aguilella, J.L. Nieva, A. Alcaraz, Ion channel activity of the CSFV p7 viroporin in surrogates of the ER lipid bilayer, Biochim. Biophys. Acta - Biomembr. 2016 (1858) 30–37, https://doi.org/10.1016/j.bbamem.2015.10.007.

[22] E. Largo, D.P. Gladue, J. Torralba, V.M. Aguilella, A. Alcaraz, M.V. Borca, J.L. Nieva, Mutation-induced changes of transmembrane pore size revealed by combined ion-channel conductance and single vesicle permeabilization analyses, Biochim. Biophys. Acta - Biomembr. 2018 (1860) 1015–1021, https://doi.org/10.1016/j.bbamem.2018.01.012.

[23] A.J. García-Sáez, M. Coraiola, M.D. Serra, I. Mingarro, P. Müller, J. Salgado, Peptides corresponding to helices 5 and 6 of Bax can independently form large lipid pores, FEBS J. 273 (2006) 971–981, https://doi.org/10.1111/j.1742-4658.2006.05123.x.

[24] G.A. Woolley, Channel-forming activity of alamethicin: Effects of covalent tethering, Chem. Biodivers. 4 (2007) 1323–1337, https://doi.org/10.1002/cbdv.200790113.

[25] M.T. Lee, W.C. Hung, F.Y. Chen, H.W. Huang, Mechanism and kinetics of pore formation in membranes by water-soluble amphipathic peptides, Proc. Natl. Acad. Sci. U. S. A. 105 (2008) 5087–5092, https://doi.org/10.1073/pnas.0710625105.

[26] E. Gazit, A. Boman, H.G. Boman, Y. Shai, Interaction of the Mammalian antibacterial peptide cecropin P1 with phospholipid vesicles, Biochemistry. 34 (1995) 11479–11488, https://doi.org/10.1021/bi00036a021.

[27] B. Hille, Ion channels of excitable membranes, third ed., Sinauer Associates Inc, Sunderland, MA, 2001. http://www.sinauer.com/ion-channels-of-excitable-membranes.html#.UvDS-CVNRd8.mendeley.

[28] T. Mehnert, A. Routh, P.J. Judge, Y.H. Lam, D. Fischer, A. Watts, W.B. Fischer, Biophysical characterization of Vpu from HIV-1 suggests a channel-pore dualism, Proteins. 70 (2008) 1488–1497, https://doi.org/10.1002/prot.21642.

[29] W.B. Fischer, H.J. Hsu, Viral channel forming proteins - Modeling the target, Biochim. Biophys. Acta - Biomembr. 2011 (1808) 561–571, https://doi.org/10.1016/j.bbamem.2010.05.014.

[30] A. Ridi, E. Scalas, A. Gliozzi, Noise measurements in bilayer lipid membranes during electroporation, Eur. Phys. J. E. 2 (2000) 161, https://doi.org/10.1007/s101890050050.

[31] T. Kotnik, L. Rems, M. Tarek, D. Miklavčič, Membrane Electroporation and Electropermeabilization: Mechanisms and Models, Annu. Rev. Biophys. 48 (2019) 63–91, https://doi.org/10.1146/annurev-biophys-052118-115451.

[32] R.M. Pielak, J.J. Chou, Influenza M2 proton channels, Biochim. Biophys. Acta - Biomembr. 2011 (1808) 522–529, https://doi.org/10.1016/j.bbamem.2010.04.015.

[33] E. Steinmann, F. Penin, S. Kallis, A.H. Patel, R. Bartenschlager, T. Pietschmann, Hepatitis C virus p7 protein is crucial for assembly and release of infectious

virions, PLoS Pathog. 3 (2007), https://doi.org/10.1371/journal.ppat.0030103 e103.

[34] B. Neumcke, 1/f noise in membranes, Biophys. Struct. Mech. 4 (1978) 179–199, https://doi.org/10.1007/BF02426084.

[35] [35] S.M. Bezrukov, I. Vodyanoy, Noise in biological membranes and relevant ionic systems, (2009) 375–399. https://doi.org/10.1021/ba-1994-0235.ch017.

[36] G.C. Fadda, D. Lairez, G. Zalczer, Fluctuations of ionic current through lipid bilayers at the onset of peptide attacks and pore formation, Phys. Rev. Lett. 103 (2009) 1–4, https://doi.org/10.1103/PhysRevLett.103.180601.

[37] P. Waduge, R. Hu, P. Bandarkar, H. Yamazaki, B. Cressiot, Q. Zhao, P.C. Whitford, M. Wanunu, Nanopore-based measurements of protein size, fluctuations, and conformational changes, ACS Nano. 11 (2017) 5706–5716, https://doi.org/10.1021/acsnano.7b01212.

[38] A. Fragasso, S. Schmid, C. Dekker, Comparing current noise in biological and solid-state nanopores, ACS Nano. 14 (2020) 1338–1349, https://doi.org/10.1021/acsnano.9b09353.

[39] M. Zorkot, R. Golestanian, D.J. Bonthuis, The power spectrum of ionic nanopore currents: the role of ion correlations, Nano Lett. 16 (2016) 2205–2212, https://doi.org/10.1021/acs.nanolett.5b04372.

[40] G. van Meer, D.R. Voelker, G.W. Feigenson, Membrane lipids: where they are and how they behave, Nat. Rev. Mol. Cell Biol. 9 (2008) 112–124, https://doi.org/10.1038/nrm2330.

[41] M. Montal, P. Mueller, Formation of bimolecular membranes from lipid monolayers and a study of their electrical properties, Proc. Natl. Acad. Sci. U. S. A. 69 (1972) 3561–3566 (accessed December 18, 2013) http://www.pubmedcentral.nih.gov/articlerender.fcgi?artid=389821&tool=pmcentrez&rendertype=abstract.

[42] L. Kullman, P. Gurnev, M. Winterhalter, S. Bezrukov, Functional subconformations in protein folding: Evidence from single-channel experiments, Phys. Rev. Lett. 96 (2006), https://doi.org/10.1103/PhysRevLett.96.038101 038101.

[43] C. Wen, S. Zeng, K. Arstila, T. Sajavaara, Y. Zhu, Z. Zhang, S.L. Zhang, Generalized noise study of solid-state nanopores at low frequencies, ACS Sens. 2 (2017) 300–307, https://doi.org/10.1021/acssensors.6b00826.

[44] C. Tasserit, A. Koutsioubas, D. Lairez, G. Zalczer, M.-C. Clochard, Pink noise of ionic conductance through single artificial nanopores revisited, Phys. Rev. Lett. 105 (2010), https://doi.org/10.1103/PhysRevLett.105.260602 260602.

[45] E. Rigo, Z. Dong, J.H. Park, E. Kennedy, M. Hokmabadi, L. Almonte-Garcia, L. Ding, N. Aluru, G. Timp, Measurements of the size and correlations between ions using an electrolytic point contact, Nat. Commun. 10 (2019) 2382, https://doi.org/10.1038/s41467-019-10265-2.

[46] Z.S. Siwy, A. Fuliński, Origin of 1/f(alpha) noise in membrane channel currents, Phys. Rev. Lett. 89 (2002), https://doi.org/10.1103/PhysRevLett.89.158101 158101.

[47] S.M. Bezrukov, M. Winterhalter, Examining noise sources at the single-molecule level: 1/f noise of an open maltoporin channel, Phys. Rev. Lett. 85 (2000) 202–205, https://doi.org/10.1103/PhysRevLett.85.202.

[48] P. Bak, C. Tang, K. Wiesenfeld, Self-organized criticality: An explanation of the 1/ f noise, Phys. Rev. Lett. 59 (1987) 381–384, https://doi.org/10.1103/PhysRevLett.59.381.

[49] R.F. Voss, J. Clarke, 1F noise from systems in thermal equilibrium, Phys. Rev. Lett. 36 (1976) 42–45, https://doi.org/10.1103/PhysRevLett.36.42.

[50] M.S. Keshner, 1/f Noise, Proc. IEEE. 70 (1982) 212–218, https://doi.org/10.1109/PROC.1982.12282.

[51] D.P. Hoogerheide, S. Garaj, J.A. Golovchenko, Probing surface charge fluctuations with solid-state nanopores, Phys. Rev. Lett. 102 (2009), https://doi.org/10.1103/PhysRevLett.102.256804 256804.

[52] S. De, R. Basu, Confirmation of membrane electroporation from flicker noise, Phys. Rev. B - Condens. Matter Mater. Phys. 61 (2000) 6689–6691, https://doi.org/10.1103/PhysRevB.61.6689.

[53] M.R. Powell, I. Vlassiouk, C. Martens, Z.S. Siwy, Nonequilibrium 1/f noise in rectifying nanopores, Phys. Rev. Lett. 103 (2009), https://doi.org/10.1103/PhysRevLett.103.248104 248104.

[54] R.M.M. Smeets, U.F. Keyser, N.H. Dekker, C. Dekker, Noise in solid-state nanopores, Proc. Natl. Acad. Sci. U. S. A. 105 (2008) 417–421, https://doi.org/10.1073/pnas.0705349105.

[55] F. Wohnsland, R. Benz, 1/f-Noise of open bacterial porin channels, J. Membr. Biol. 158 (1997) 77–85 (accessed December 18, 2013) http://www.ncbi.nlm.nih.gov/pubmed/9211723.

[56] E. van den Brink-van der Laan, J.A. Killian, B. de Kruijff, Nonbilayer lipids affect peripheral and integral membrane proteins via changes in the lateral pressure profile., Biochim. Biophys. Acta. 1666 (2004) 275–88. https://doi.org/10.1016/j.bbamem.2004.06.010.

[57] R.H. Swendsen, Dynamics of random sequential adsorption, Phys. Rev. A. 24 (1981) 504–508, https://doi.org/10.1103/PhysRevA.24.504.

[58] O. Michielin, G. Vergères, J.J. Ramsden, Myristoylation-induced compaction of a membrane-binding protein, J. Am. Chem. Soc. 121 (1999) 6523–6526, https://doi.org/10.1021/ja990239j.

[59] B.M. Manzi, M. Werner, E.P. Ivanova, R.J. Crawford, V.A. Baulin, Simulations of protein adsorption on nanostructured surfaces, Sci. Rep. 9 (2019) 1–13, https://doi.org/10.1038/s41598-019-40920-z.

[60] A. Luganini, G. Di Nardo, L. Munaron, A. Gilardi, A. Fiorio Pla, G. Gribaudo, Human cytomegalovirus US21 protein is a viroporin that modulates calcium homeostasis and protects cells against apoptosis, Proc. Natl. Acad. Sci. 115 (2018) E12370–E12377, https://doi.org/10.1073/pnas.1813183115.

[61] C. StGelais, T.J. Tuthill, D.S. Clarke, D.J. Rowlands, M. Harris, S. Griffin, Inhibition of hepatitis C virus p7 membrane channels in a liposome-based assay system, Antiviral Res. 76 (2007) 48–58, https://doi.org/10.1016/j.antiviral.2007.05.001.